Portable Self-propelled Force Feedback Device

Ayaka Fukasawa, Riho Taniguchi, Takumi Sato, Shoichi Hasegawa
Tokyo Institute of Technology ,Japan

***Abstract*—One of the purposes of the force feedback device for virtual reality is to prevent the user's body from penetrating virtual objects and/or to facilitate object manipulations. However, as such devices are fixed, their workspace is confined to their movable range. To address this limitation, we propose a lightweight and portable device that is grounded and capable of presenting force but has no workspace constraints. To evaluate the performance of the proposed device, we measured hand trajectories and presentation forces while presenting objects in the shape of a wall, table, and sphere.**

***Index Terms*—Haptic, grounded, portable, virtual reality, force feedback**

I. Introduction

Various applications including teleoperation and surgical simulation utilize force feedback devices that can apply force to the user. In virtual reality (VR), force feedback significantly enhances the user's perception of virtual objects and their ability to manipulate them. However, most conventional force feedback devices for large and steady external feedback forces are fixed to the ground, resulting in a limited workspace. An expanded workspace could be achieved by a device that is either large and heavy or wearable and that provides only relative force from the wearing position. This study proposes a lightweight self-propelled device that can provide a large force through a grounded and simple mechanism. The device is capable of providing grounded force feedback to the user in the HMD VR environment and preventing the user from penetrating virtual objects.

This device is suitable for applications involving interaction with objects. For example, it can simulate walls and objects and provide force feedback for pushing, pulling, and lifting actions, including opening and closing doors or carrying objects. Additionally, since the range of motion of the device is not limited, it can be used for applications such as exploring a maze or walking a dog.

II. Previous Research

This section describes the related research on force feedback devices that can provide both cutaneous and kinesthetic sensations; this study focuses specifically on the latter. In addition, force feedback devices can be broadly classified into two types: wearable and grounded.

Wearable devices present a sense of force to the part of the body. For example, a device worn along the hand exoskeleton provides tactile feedback on grasping maneuvers [1] [2]. However, they have a limitation in that they can only present internal forces between the wearing and presenting parts of the body and cannot present the external forces necessary to constrain the motion of the presenting part. While the devices can present force between the fingers, wrists, and palms, they cannot present a load on the entire body.

Grounded devices can transmit external forces to the user's body by transmitting them to the ground through the device. However, many installation-type devices are fixed to the ground, resulting in a limited workspace. Consequently, methods to extend the range of motion are also under investigation.

PHANToM [3] and SPIDAR [4] are grounded devices that can provide highly accurate force feedback and fine motion. Similarly, the HaptionVituose6D [5] can present a large force in six degrees of freedom (DOF). However, the range of motion is limited for all of these devices.

A proposed solution to address this limitation is to create a force feedback device with a movable area of the same size as the workspace [6]. However, such a device would be massive and would limit the users and use cases [7].

Other solutions have been proposed to increase the range of motion of the device. Gosselin et al. hung the Haption Virtuose 6D [5], a 6-DOF grounded device, from the ceiling and moved it by sliding it along a beam [8]. Similarly, Ueberle et al. [9] proposed the VISHARD 10, a 10-DOF controlled robotic arm that eliminated the workspace specificity of 6-DOF devices. However, in both cases, the installation of the device restricted the available workspace. Other approaches have suggested integrating two haptic interfaces. Anthony et al. integrated a grounded 6-DOF force-feedback arm with a hand-mounted haptic interface [10]. They proposed integrating the two devices when the grounded device is within reach and relying solely on the hand-worn device to provide force feedback when the user moves beyond the range of the grounded device. However, this approach only provides force to the wearable device in areas beyond the grounded device's reach and presents varying force feedback depending on the location of use.

To provide an unlimited range of motion, a potential solution is to integrate an installed device with a mobile robot. Nitzsche et al. demonstrated the feasibility of a force-haptic interface by combining an omnidirectional mobile base with the Sensable Phantom Premium 1.0 device [11]. They named this interface the Mobile Haptic Interface (MHI) and demonstrated that it could be moved to any location. This approach was also used for VISHARD7 [12], a modification of VISHARD10 [9]. Han et al. developed a control system for the MHI that enables omnidirectional movement using mecanum wheels as a mobile base [13]. Ryan et al. integrated hardware and software to use the Haption Virtuose™ 6D on a

mobile base [14]. However, this approach involves mounting the device on a mobile robot, making it large and heavy.

In contrast to these approaches, the proposed ground-based device utilizes a simple two-wheeled driving unit that, when combined with a grip, enables tactile presentation of force through the control of three motors. Unlike installation-type devices, there are no workspace limitations on this driving unit. Additionally, due to its lightweight design and straightforward mechanism, the device is highly portable and can present continuous external force, unlike non-grounded devices except for those that provide such feedback through the air [15].

III. System Overview

This section describes the proposed device design and the static analysis.

A. Proposal

The proposed device overcomes the workspace limit by utilizing a driving unit. The mechanism applies torque instead of a vertical force to the hand to keep the mechanism simple. Therefore, the range of motion is unrestricted horizontally but limited vertically by the length of the pipe.

To prevent the hand from penetrating the object during locomotion, the force in the rear direction should be stronger than in the right/left direction. Therefore, two tires are grounded, and forces in the front/rear direction are presented by translational forces driven in the same direction. Forces in the right/left direction are created by the torque generated when driving in the opposite direction. While the driving unit can generate a torque in the pitch direction to present vertical force and torque independently (e.g. by using four wheels), this study avoids making the driving unit larger and accepts the side effect of pitch axis torque when presenting the vertical force.

B. Device design

The hardware configuration of the proposed device is shown in Figure 1. As the driving unit moves in relation to the hand, the device's posture is automatically determined. Therefore, we focus solely on the force and torque generated by the proposed device.

The two wheels are driven independently; their combined action generates the front-rear force, which is then transmitted to the grip through the pipe. The torque around the vertical axis (y-axis) which is centered on the driving unit is generated by the difference in forces on the wheels, resulting in a translational force in the right/left direction (x-axis) at the hand position. The vertical force is produced by the gravitational force of the device and the normal force from the floor. However, the force exerted by the pipe on the grip in the YZ plane is greater in the vertical (y-axis) direction than in the forward-backward (z-axis) direction as the hand moves upward and the pipe becomes more upright. This effect can be mitigated by increasing the length of the pipe to bring it closer to the horizontal position.

The pipe, located further than the one connecting the grip and the driving unit, is driven up and down by a motor in the center of the driving unit to generate torque at the tip of the grip. The motor's rotation is converted into vertical motion by a reduction motion conversion mechanism using a screw and wire which mimics that of the PHANToM's reducer [3].

C. Static Analysis of the Device

This section presents the statics of the proposed device for each axis of the rigid bodies of the grip and driving unit. The notations for the parameters in the analysis are listed below.

- Frictional forces on wheels : f_1, f_2
- Torque applied to grip by motor located at center : T
- Force applied to hand : F
- Torque in the x-axis direction applied to grip : T_h
- Joint force between grip and pipe : C
- Overall mass of device : m
- Gravitational acceleration : g
- Normal force from ground : N
- Length from installation surface to grip joint : l_1
- Length of grip : l_2
- Length between wheels : l_3
- Angle of pipe to the horizon : φ
- Angle of grip relative to the horizon : θ

The angle is positive in a clockwise direction in the figure. To ensure safe operation and ease of control, the driving unit must always be placed at the far side of the grip so that θ cannot exceed $90°$. Additionally, φ cannot exceed θ to prevent overlapping of the parallel linked pipes.

The equations for determining the equilibrium of forces for the grip and the driving unit are shown below. For the horizontal equilibrium of forces, the grip side is expressed in Equation (1) and the driving unit side is expressed in Equation (2).

$$C_z - F_z = 0 \tag{1}$$

$$-C_z + (f_1 + f_2) = 0 \tag{2}$$

For the vertical equilibrium of forces, the grip side is expressed in Equation (3) and the driving unit side is expressed in Equation (4).

$$C_y - F_y = 0 \tag{3}$$

$$-C_y + N - mg = 0 \tag{4}$$

For the equilibrium of torques around the x-axis, the grip side is expressed in Equation (5) and the driving unit side is expressed in Equation (6).

$$T - T_h + C_y l_2 \cos\varphi + C_z l_2 \sin\varphi = 0 \tag{5}$$

$$-T + (N - mg) l_1 \cos\theta + (f_1 + f_2) l_1 \sin\theta = 0 \quad . \tag{6}$$

From Equations (3), (4), (6),

$$F_y = \frac{T}{l_1 \cos\theta} - (f_1 + f_2) \tan\theta. \tag{7}$$

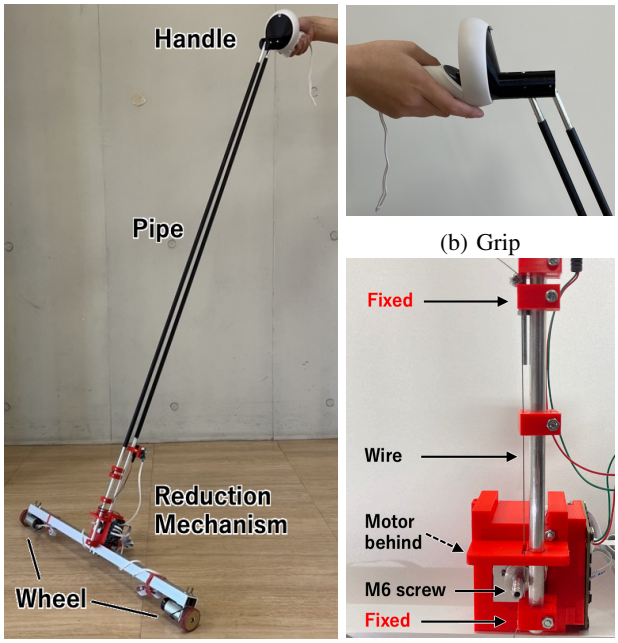

(a) Overall view (b) Grip (c) Reduction mechanism

Fig. 1. Device

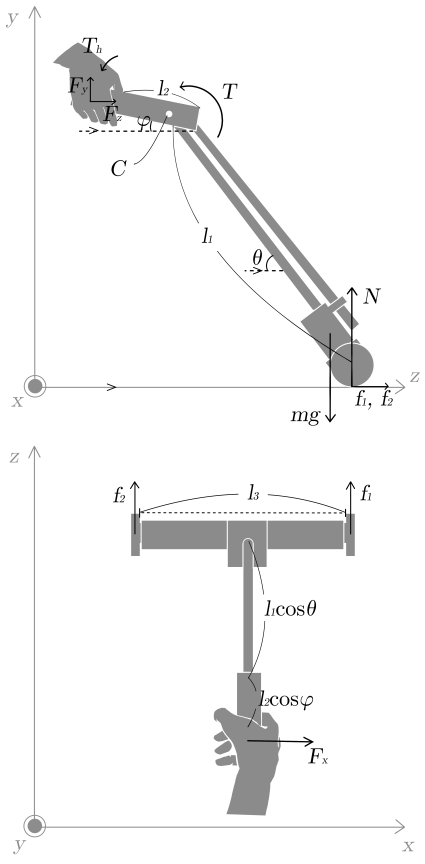

Fig. 2. Statics analysis of the proposed device

The hand is subjected to the torque T_h around the x-axis.

$$T_h = T(1 + \frac{l_2 \cos\varphi}{l_1 \cos\theta}) + (f_1 + f_2) l_2 (\sin\varphi - \tan\theta \cos\varphi) \quad (8)$$

The equilibrium of torques around the y-axis is expressed in Equation (9), with the clockwise direction being positive, as shown in Figure 2.

$$(f_1 - f_2)\frac{l_3}{2} - F_x(l_1 \cos\theta + l_2 \cos\varphi) = 0. \quad (9)$$

From the above,

$$F_x = \frac{(f_1 - f_2) l_3}{2(l_1 \cos\theta + l_2 \cos\varphi)}. \quad (10)$$

D. Implement

To facilitate the vertical force, the pipe connecting the driving unit and the grip is made of CFRP, which is a lightweight material. When upright, the height of the grip l_1 is 1,355 mm.

Posture tracking of the grip is performed using the Meta Quest's system, and the hand position is tracked by the right controller of Meta Quest2. The part of the grip that connects the controller and the two pipes is made of ABS using a 3D printer. The distance l_2 between the back end of the grip and the joint axis is 170 mm, and the distance l_3 between the tires is 632 mm.

The mechanism for presenting torque around the pitch axis to the grip (Figure 1c) involves an M6 screw serving as the motor shaft, around which a wire is wound and both ends are attached to the back of the movable pipe. Torque is presented to the grip by rotating the motor and moving the pipe up and down via the wire. The motors used in this device are RE-max 29 ϕ 29 mm from Maxon International Ltd. The total weight of the device is 1.45 kg.

Motor control ICs capable of current control are used to drive the motors since the torque generated by a motor is proportional to the current. The PWM outputs from the microcontroller (PIC32MK0512MCJ by Microchip Technology Inc.) are converted to voltages with RC low-pass filters for the current control inputs of the motor driver (ICs DRV8434E by Texas Instruments Inc.) A 24 V, 5 A AC adapter is used as the power supply for the motor driver. The microcontroller is connected to a PC via a 2M baud UART through a USB-serial converter to update current values at a frequency of 1,000 Hz or higher.

E. Device Control

A virtual environment was created using Unity version 2021.3.3f1, and physics simulation and VR coupling were performed using Springhead [16].

The coefficient of static friction between the wall, table, and hand is 0.5, while the coefficient of kinetic friction is 0.35. The coefficients of static and kinetic friction for the ball are both 0.

To calculate the force applied to the motors, we first obtain the forces F_x, F_y, F_z from the virtual coupling. From Equations (1) and (2),

$$F_z = f_1 + f_2 \tag{11}$$

From Equation (10)

$$f_1 - f_2 = \frac{2F_x(l_1 \cos\theta + l_2 \cos\varphi)}{l_3}. \tag{12}$$

So that

$$f_1 = \frac{F_z}{2} + \frac{F_x}{l_3}(l_1 \cos\theta + l_2 \cos\varphi)$$
$$f_2 = \frac{F_z}{2} - \frac{F_x}{l_3}(l_1 \cos\theta + l_2 \cos\varphi).$$

Regarding that the changes in θ, φ are negligible, we choose $k \equiv (l_1 \cos\theta + l_2 \cos\varphi)/l_3 = 0.3$ and we obtain

$$f_1 = \frac{F_z}{2} + kF_x, \quad f_2 = \frac{F_z}{2} - kF_x. \tag{13}$$

Also, by approximating Equation (7) with $\theta = 0$, we obtain

$$T = F_y l_1. \tag{14}$$

IV. Evaluation

To evaluate the performance of the proposed device, we first measured the force it presented. We used a weight scale to measure the force at both the maximum and half current command values. The presented force was linearly proportional to the current command value, so we used this measured value for conversion. The maximum front/rear force exerted by a wheel was 1.7 N and the torque in the pitch direction applied to the grip was -0.119 ± 0.357 N·m, including torque from grip weight.

Next, we evaluate the functionality of the device by presenting virtual objects.

A. Experimental setup

The objectives of this experiment are to determine whether the trajectory of the hand follows the shape of the virtual object using the proposed device and to evaluate whether the device can properly present force. To evaluate whether the device can handle force presentation in various directions, we prepared three walls at different angles, a table, and a sphere with a diameter of 0.5 m suspended in the air in a virtual environment.

B. Procedure

As depicted in Figure 2, the device was placed in the direction of the z-axis of the virtual environment. We alternately touched and released the device to measure the hand trajectory and the force presented by the device. Additionally, a 0.3 m square frame was displayed on the wall and table to evaluate the ability of the device to trace these neatly and present frictional force effectively.

Figure 3 shows the placement of the three walls in front, at a 45-degree angle to the right, and to the right, respectively. Black squares were used on the walls for tracing.

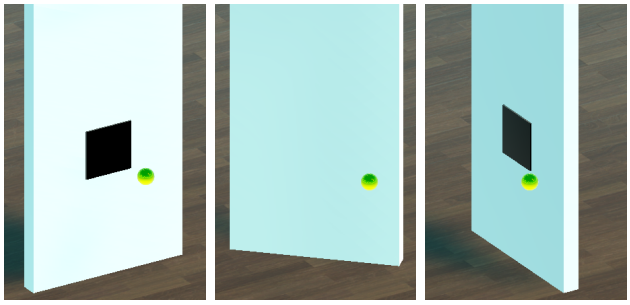

(a) Front (b) 45-degree (c) Right

Fig. 3. Wall and Hand's Sphere

C. Result

To analyze the results of touching the walls or table, graphs summarizing the distance from grip to surfaces and the force presented are shown in Figure 4. The graphs show both force and distance on the same axis, with force (N) and torque (N·m) graphed on the primary axis and distances (m) on the secondary axis. The horizontal axis of all the time-series data represents time (s). Note that T represents a value that includes not only the torque due to the reduction mechanism but also the weight of the grip.

Next, graphs are presented to show the results of tracing a wall or a table when each is touched. Figure 5 shows the tracing trajectory on each surface, Figure 6 shows trajectory coordinates time-series, and Figure 7 shows the time series of forces and distance from grip to surfaces presented to the device during the experiment.

Finally, graphs are presented to show the results of tracing a curved surface. Two graphs depict tracings of the upper side of the sphere from front to back and left to right. Another graph depicts a tracing of the lower side of the sphere from back to front. Figure 8 represents the trajectory for each direction of movement.

D. Discussion

Regarding the difference in accuracy based on the position of contact with the object, in the case of a collision with the object, we can consider that the reaction force of the collision could be presented without any change in the coordinates of the collision direction, as shown in Figure 4. For the presentation of the shape of the wall, it can be seen in Figure 6 that when tracing the planes of the virtual object, the amount of penetration into the objects is small and remains constant, and the feedback force properly presents the planes. In contrast, for the tracing of the upper hemisphere, as shown in Figure 8a, the amount of penetration increases up to approximately 0.3 to 0.6 m when the surface normal comes to $(0, y, z)(y, z > 0)$ in the coordinate system shown in Figure 2.

We consider the cause of this result to be as follows: when the surface normal is in the positive orientation of the y- and z-axis ($(0, y, z)(y, z > 0)$), the driving unit pulls the grip in the direction of the pipe to provide the presenting force F_z. As a result, a downward force is exerted on the grip, which

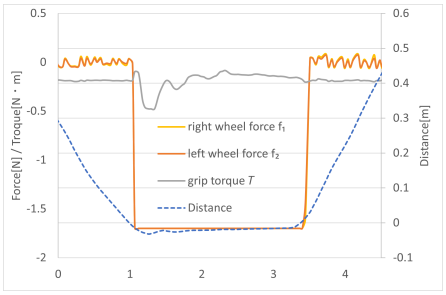

(a) Forward wall

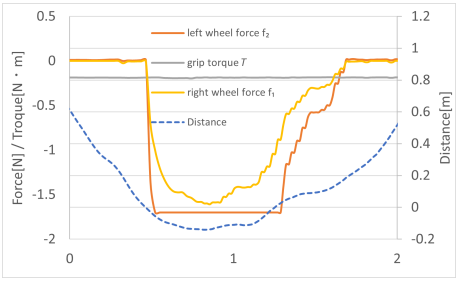

(b) 45-degree wall

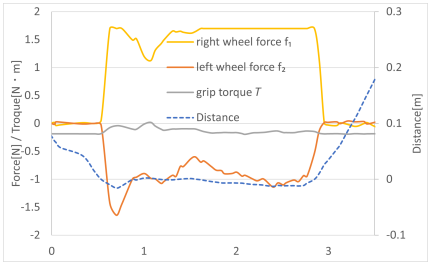

(c) Right wall

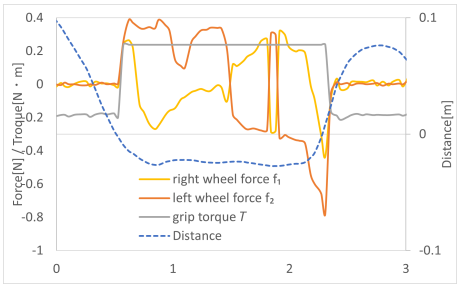

(d) Table from top

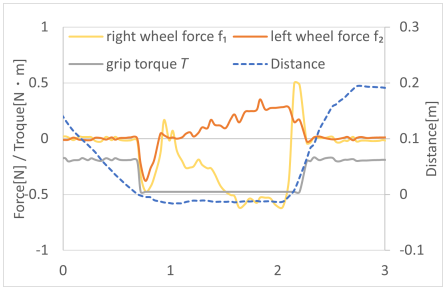

(e) Table from bottom

Fig. 4. Time-series of distance from grip to surfaces and forces and torque for touching planes

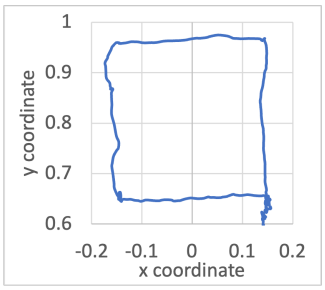

(a) Forward Wall

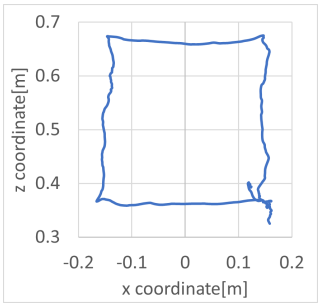

(b) Table

Fig. 5. Trajectory for tracing planes

balances the upward force F_y, generated by the torque T at the joint between the grip and pipe. This result makes it difficult for the user to feel the upward force, and consequently the amount of penetration increases.

Furthermore, we observed more penetration in the lower hemisphere (Figure 8c) than in the upper hemisphere (Figure 8a); this is likely due to the limited range of motion of the grip. Of note, when the grip traced the lower hemisphere, the tilt of the grip reached the upper limit of the device, making it impossible to present force in the vertical direction.

Furthermore, there were upper and lower limits to the motor's power. For example, as shown in Figure 4b, the force exerted on the right wheel represents the lower limit, beyond which no further force can be exerted because the right/left direction is presented by the positive/negative difference in the front/rear direction of the wheels. This limitation can likely be addressed by modifying the design to generate a translational force in the right/left direction by attaching a rotational axis

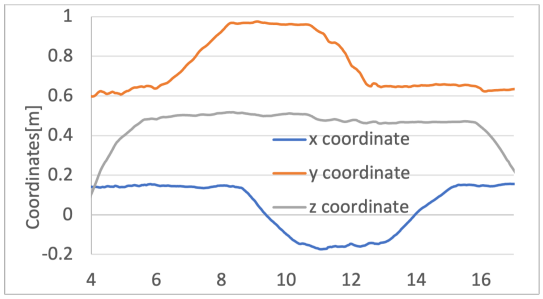

(a) Front Wall

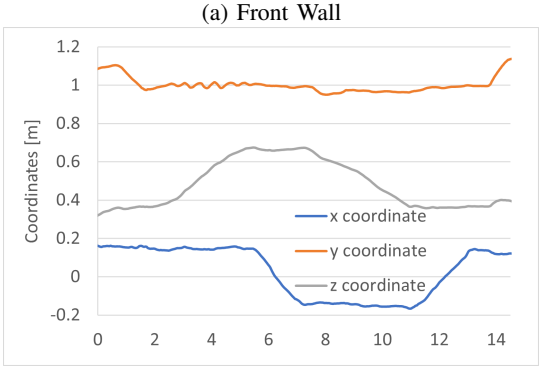

(b) Table

Fig. 6. Trajectory coordinates time-series for Tracing Planes

capable of producing torque in the center of the driving unit.

Based on the above results, force feedback can help reduce penetration, but oblique surfaces can present more challenges depending on their orientation. Additionally, the amount of penetration increases when the device's range of motion exceeds its limits.

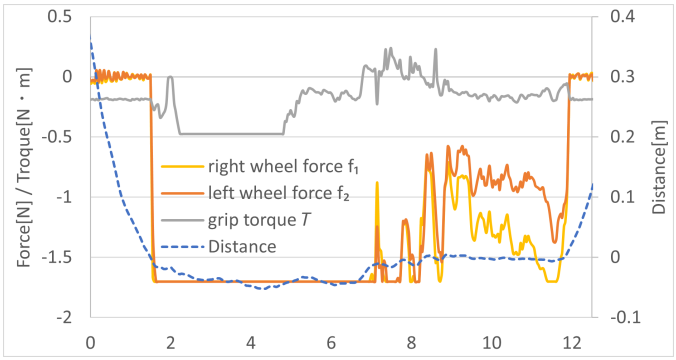

(a) Forward Wall

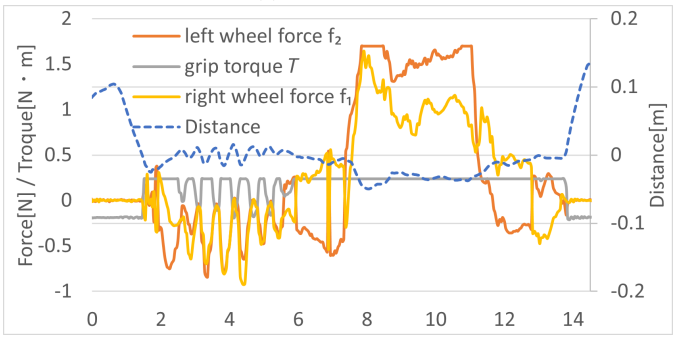

(b) Table

Fig. 7. Time-series of distance from grip to surfaces and forces and torque for tracing planes

Finally, our results suggest that friction can be presented because forces are also generated from directions other than the contact normal, as shown in Figures 6 and 7. For instance, when tracing the square in Figure 6a, from 2 to 4 seconds, the device moves toward the y-axis direction and generates a frictional force (torque T which presents a vertical force). (Figure 7a).

V. Limitation

The grip in the proposed mechanism only rotates around the pitch axis, restricting the user from freely rotating the orientation of the grip. Therefore, additional rotation axes around the yaw and roll axes are required to achieve free operation in a VR environment. In the proposed mechanism, the orientation of the traveling part around the yaw axis is determined passively, which makes it difficult to maintain the positional relationship between the mechanism and the user depending on the path of movement of the grips. To solve this issue, a driven rotation around the yaw axis in the center of the driving unit is needed to control the orientation of the pipe and the driving unit independently. In addition, consideration for controlling non-holonomics will be needed.

In the proposed mechanism, the presentation of vertical force comes with torque, but the effects on the sensation were not evaluated. It was not possible to use a stiff spring in the virtual coupling for the proposed device due to the extended period of position measurement. Therefore, it is recommended

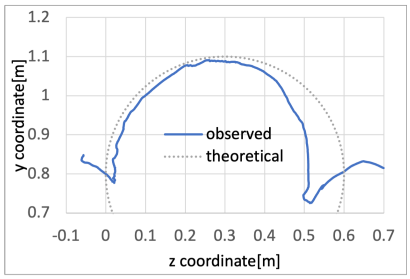

(a) Upper hemisphere front to back

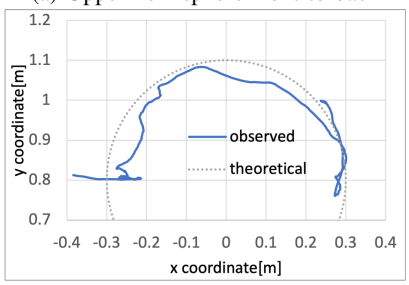

(b) Upper hemisphere left to right

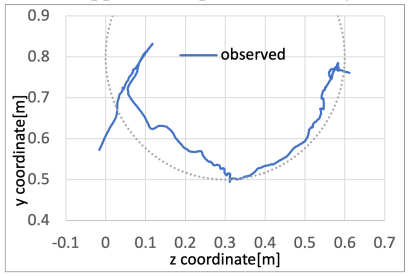

(c) Lower hemisphere back to front

Fig. 8. Trajectory coordinates time-series for tracing spheres

to mechanism with an IMU to speed up the measurement and control loop.

VI. Conclusion

This paper proposes a simple mechanism for a grounded haptic interface that can exert an external force on the user without any movable range limitations. To investigate the device's performance and functionality, shape presentation experiments were conducted, and the results showed that force feedback reduced the amount of penetration. However, for oblique surfaces, the amount of penetration increased depending on the normal direction compared to the walls and table. A noted limitation is that presenting an upward force was challenging when the surface normal was in an up-outward direction.

Acknowledgments

We would like to express our gratitude to the members of the laboratory for their invaluable cooperation in conducting this research. This work was supported by JSPS KAKENHI Grant Number JP23H03432.

REFERENCES

[1] I. Choi, E. W. Hawkes, D. L. Christensen, C. J. Ploch, and S. Follmer, "Wolverine: A wearable haptic interface for grasping in virtual reality," in *2016 IEEE/RSJ International Conference on Intelligent Robots and Systems (IROS)*. IEEE, 2016, pp. 986–993.

[2] M. Fontana, S. Fabio, S. Marcheschi, and M. Bergamasco, "Haptic hand exoskeleton for precision grasp simulation," *Journal of Mechanisms and Robotics*, vol. 5, no. 4, p. 041014, 2013.

[3] T. H. Massie and J. K. Salisbury, "The phantom haptic interface: A device for probing virtual objects," in *Proceedings of the ASME winter annual meeting, symposium on haptic interfaces for virtual environment and teleoperator systems*, vol. 55, no. 1. Chicago, IL, 1994, pp. 295–300.

[4] M. Sato, "Spidar and virtual reality," in *Proceedings of the 5th Biannual World Automation Congress*, vol. 13. IEEE, 2002, pp. 17–23.

[5] "Haption 2019 Scale1," http://www.nihonbinary.co.jp/Products/VR/Haptic/Haption/Virtuose_6D_TAO.html.

[6] J. Perret and L. Dominjon, "The inca 6d: a commercial stringed haptic system suitable for industrial applications," in *Joint Virtual Reality Conference, Springer Tracts in Advanced Robotics*, 2009.

[7] F. Gosselin, C. Andriot, J. Savall, and J. Martín, "Large workspace haptic devices for human-scale interaction: A survey," in *Haptics: Perception, Devices and Scenarios: 6th International Conference, EuroHaptics 2008 Madrid, Spain, June 10-13, 2008 Proceedings 6*. Springer, 2008, pp. 523–528.

[8] F. Gosselin, C. Andriot, F. Bergez, and X. Merlhiot, "Widening 6-dof haptic devices workspace with an additional degree of freedom," in *Second Joint EuroHaptics Conference and Symposium on Haptic Interfaces for Virtual Environment and Teleoperator Systems (WHC'07)*. IEEE, 2007, pp. 452–457.

[9] M. Ueberle, N. Mock, and M. Buss, "Vishard10, a novel hyper-redundant haptic interface," in *12th International Symposium on Haptic Interfaces for Virtual Environment and Teleoperator Systems, 2004. HAPTICS'04. Proceedings.* IEEE, 2004, pp. 58–65.

[10] A. Steed, S. Friston, V. Pawar, and D. Swapp, "Docking haptics: extending the reach of haptics by dynamic combinations of grounded and worn devices," in *Proceedings of the 26th ACM Symposium on Virtual Reality Software and Technology*, 2020, pp. 1–11.

[11] N. Nitzsche, U. D. Hanebeck, and G. Schmidt, "Mobile haptic interaction with extended real or virtual environments," in *Proceedings 10th IEEE International Workshop on Robot and Human Interactive Communication. ROMAN 2001 (Cat. No. 01TH8591)*. IEEE, 2001, pp. 313–318.

[12] A. Peer, Y. Komoguchi, and M. Buss, "Towards a mobile haptic interface for bimanual manipulations," in *2007 IEEE/RSJ International Conference on Intelligent Robots and Systems*. IEEE, 2007, pp. 384–391.

[13] K.-L. Han, O. K. Choi, I. Lee, I. Hwang, J. S. Lee, and S. Choi, "Design and control of omni-directional mobile robot for mobile haptic interface," in *2008 International Conference on Control, Automation and Systems*. IEEE, 2008, pp. 1290–1295.

[14] R. A. Pavlik, J. M. Vance, and G. R. Luecke, "Interacting with a large virtual environment by combining a ground-based haptic device and a mobile robot base," in *International Design Engineering Technical Conferences and Computers and Information in Engineering Conference*, vol. 55867. American Society of Mechanical Engineers, 2013, p. V02BT02A029.

[15] T. Sasaki, R. S. Hartanto, K.-H. Liu, K. Tsuchiya, A. Hiyama, and M. Inami, "Leviopole: mid-air haptic interactions using multirotor," in *ACM SIGGRAPH 2018 Emerging Technologies*, 2018, pp. 1–2.

[16] Y. Tazaki and S. D. Team, "Springhead libraries, new repository with history from 2004," https://github.com/Springhead/Springhead, 2023.